FISEVIER

Contents lists available at ScienceDirect

Journal of Materials Processing Tech.

journal homepage: www.elsevier.com/locate/jmatprotec



Ultrasonic resistance welding of TRIP-780 steel

U.H. Shah, X. Liu*

Department of Materials Science & Engineering, The Ohio State University, Columbus, OH, 43201, USA



ARTICLE INFO

Associate Editor: C.H. Caceres Keywords: Ultrasonic resistance welding Power ultrasonic Resistance spot welding Tempered martensite

ABSTRACT

A hybrid ultrasonic resistance spot welding process is developed, which integrates high-power ultrasonic vibrations into conventional resistance spot welding process. Weldability of galvanized transformation induced plasticity (TRIP-780) steel is studied based on this process. Ultrasonic resistance welds showed nugget pullout failure mode and more ductility compared with conventional resistance spot welds. Optical and scanning electron microscopic analysis revealed the refined microstructure in the fusion zone and heat affected zone of ultrasonic resistance welds. Coalesced bainite is present the fusion zone of conventional resistance spot welds while possible tempered martensite and feathery bainite is observed in ultrasonic resistance welds, which accounts for their higher ductile behavior.

1. Introduction

With the growing amount of advance high strength steels (AHSS) used in vehicle structures for light weighting, economical and reliable welding techniques are highly desired. The multiphase microstructure on one hand provides AHSS with unique mechanical properties. On the other hand, it can be relatively challenging to achieve satisfying welds, due to the associated temperature and stress fields in conventional welding process, for example, resistance spot welding (RSW). This would completely change the original multiphase microstructure and may require additional post processing steps to attain required properties. Pouranvari and Marashi (2011) reported RSW welds made on AHSS are more prone to deficiencies, such as shrinkage voids. Dancette et al. (2011) described the interfacial debonding of RSW welds as a combined result of martensite formation in the fusion zone, softening in the heat affected zone (HAZ) and elemental segregation. Rezayat et al. (2016) attributed the drop of hardness in HAZ to the tempering of martensite in the original steel structure. Baltazar Hernandez et al. (2010) mentioned that this tempering is a result of diffusion of activated carbon atoms in the subcritical heat affected zone into the martensite interlath space and dislocations, followed by the cementite formation and coarsening. Pouranvari and Marashi (2013) summarized that the RSW weld strength of AHSS depends on several microstructure attributes, including fusion zone size, heat affected zone profile, and indentation depth. They reported that RSW welds on AHSS have higher tendencies towards interfacial failure mode during lap shear tensile tests, which is due to formation of voids defects and brittle products in the fusion zone. In addition, AHSS steel surface commonly contains a

coated layer for corrosion protection, which has a thickness generally in the range of 7–10 $\mu m.$ For conventional RSW, this additional coating causes uncertainties in the contact resistance, which leads to variations of weld quality. Ertek Emre et al. (2016) showed that the Zinc coating on TRIP 800 steel can reduce nugget size and accordingly joint strength. Lin et al. (2018) reported that the galvanized zinc layer narrowed the weldability lobe for mild steel.

To address these potential issues and enhance capabilities of conventional RSW for welding galvanized TRIP steel, in this study, a hybrid ultrasonic resistance welding (URW) process is developed, during which in situ ultrasonic vibrations are applied in RSW process. Highintensity ultrasonic energy has been utilized in improving manufacturing processes based on its various induced physical phenomena and effects on material mechanical behavior, as summarized by Gallego-Juárez and Graff (2015). During plastic deformation of metals in solid state, superimposed ultrasonic vibration can reduce the flow stress, which is referred to as the acousto-plastic effect and was first observed by Langenecker (1966). Jimma et al. (1998) employed this effect in deep drawing process, where a reduced forming force and improved formability was reported. Possible mechanisms of this softening phenomenon have been explained as a combined result of ultrasonic energy absorption at local lattice defects and stress superposition. When metals are in liquid state, ultrasonic vibration can induce acoustic streaming and cavitation effects, which modifies mass transport, formation, growth and collapse of bubbles. Nagarajan et al. (2006) reported that as the acoustic wave passes through the liquid, the associated alternating compression and rarefaction fields lead to microbubble formation, growth and implosions, which generates a combined

E-mail address: liu.7054@osu.edu (X. Liu).

^{*} Corresponding author.

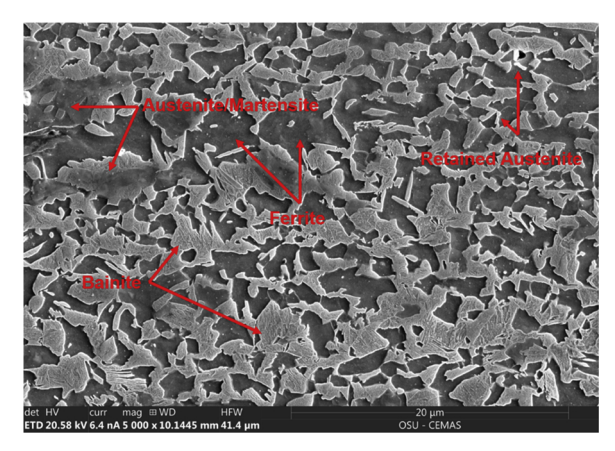


Fig. 1. SEM micrograph of the TRIP 780 sheet as received.

condition of local high temperature (5000 °C) and pressure (100 atm). Li et al. (2004) used high frequency ultrasonic waves to refine solidification structure for fabrication of metal matrix nanocomposites. Shi et al. (2018) applied ultrasonic vibration during casting of 6061 aluminum alloys and reported refined microstructure and minimized element segregation. Similarly, Qian et al. (2014) observed refined casting microstructure of AZ31 magnesium alloy by ultrasonication at a frequency of 20 kHz with the magnitude of 30 µm. Fan et al. (2012) added 20 kHz ultrasonic vibration to the electrode during gas metal arc welding. Drop detachment was enhanced, which modified the weld bead geometry and reduced weld solidification cracking. Xu et al. (2014) applied 20 kHz ultrasonic waves during the tungsten inert gas welding of magnesium. They showed the grain size of alpha magnesium has decreased from 200 μm to 50 μm in the weld microstructure. For all these melting related processes, ultrasonic energy has improved process characteristics and product properties.

The ultrasonic effects on metals in both solid and liquid states are hypothesized to improve conventional RSW process. In solid state, the softening phenomenon modifies the stress field developed around the weld nugget, which could potentially reduce weld residual stress and restrain formation of defects, such as cracks and porosities. In liquid phase, the ultrasonic vibration is anticipated to refine solidification structure, mitigate microalloy segregation, and improve joint quality. In this study, these hypotheses will be investigated. Ultrasonic effects on RSW process will be studied and the corresponding weld mechanical properties will be analyzed together with microstructure.

2. Experimental details

2.1. Material

Electrogalvanized TRIP 780 steel with the thickness of 1.6 mm and a coated Zn layer of around 7 μm is used in this study. As a reference, the as-received TRIP steel contains allotriomorphic ferrite, blocky retained austenite, dispersed bainite and small amount of martensite, shown in Fig. 1. These steel sheets are provided by ArcelorMittal and corresponding chemical compositions are listed in Table 1.

2.2. Ultrasonic resistance welding (URW) process

The experimental system for ultrasonically assisted resistance spot

Table 1Chemical compositions of the TRIP 780 steel.

TRIP-780	С	S	Mn	P	Si	Cr	Ni	Мо	Cu	V	Nb	Ti
Wt %	0.1	< 0.002	1.98	< 0.002	2.35	< 0.06	< 0.04	< 0.03	0.012	0.019	< 0.004	0.01

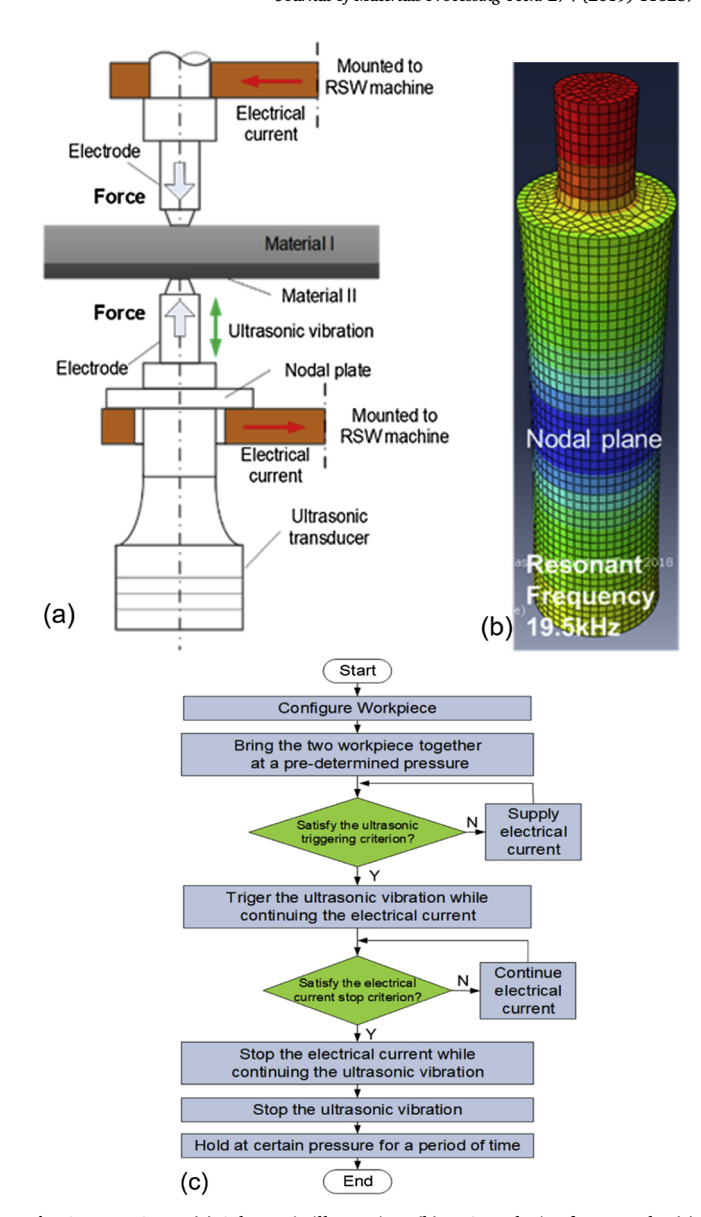


Fig. 2. URW Setup (a) Schematic illustration; (b) FEA analysis of sonotrode; (c) Flowchart of the URW process.

welding is developed, and the hybrid process is termed hereafter as Ultrasonic Resistance Welding (URW). The URW system is adapted from a conventional AC RSW machine as shown in Fig. 2(a–c). Electrical current passes from the top to the bottom electrode. The bottom electrode is directly connected to the ultrasonic transducer, serving as the sonotrode to transfer acoustic energy into the workpiece simultaneously. The total length of the bottom electrode is tuned to a certain value such that its tip surface is located at the antinodal plane and vibrates at the maximum amplitude. The natural resonation frequency of the bottom electrode is the same as that of the ultrasonic transducer (around 19.4 kHz). During URW process, the ultrasonic vibration is synchronized with the electrical current. Duration of the ultrasonic vibration is 500 ms, and the peak-to-peak vibration amplitude $V_{\rm pp}$ is 34 μm , which is measured in the unloaded condition. The AC electrical

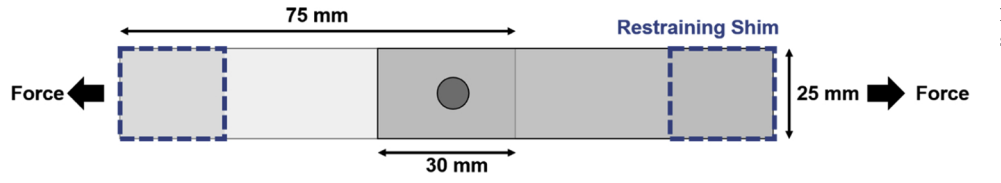


Fig. 3. Geometry of the weld specimen for lap shear tensile test.

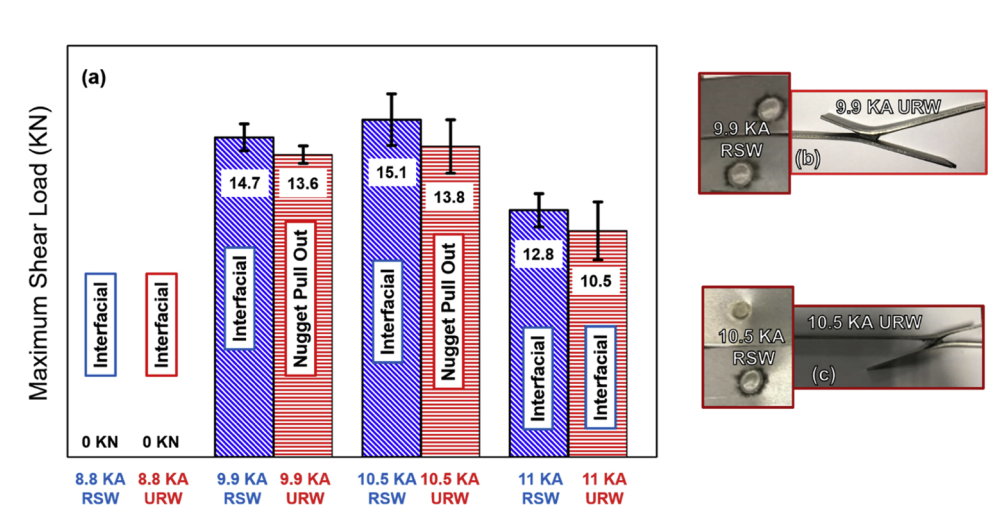


Fig. 4. 1. Weld strength and failure mode comparison between RSW and URW welds.

current is measured via a Rogowski coil, which is processed by a data acquisition and self-developed control system to determine the start-and-off time of the ultrasonic power generator. Other process parameters include AC current (60 Hz) with root mean square values of 8.8 kA, 9.9 kA, 10.5 kA and 11 kA for 20 cycles (1/3 s) and the applied welding force of 3.1 kN. RSW and URW welds are performed at the same current conditions for benchmarking and comparison.

2.3. Weld property evaluation and characterization

Lap shear tensile tests of the weld specimens are carried out by a mechanical tensile test system at a displacement rate of 1 mm/min. The long side of the weld specimen is parallel to the sheet rolling direction. Detailed geometries are provided in Fig. 3. Restraining shims are placed at the two ends of the specimen to ensure co-planar loading condition. Microstructure of the weld is characterized by light optical and scanning electron microscope (SEM). Metallurgical samples are sectioned along the weld center, ground and polished following standard preparation procedures. The samples are finally etched with 2 vol % Nital solution to reveal different steel phases. Vickers microhardness maps were measured across the weld area, including weld nugget, heat affetcted zone and base metal. The hardness measurements are performed with a load of 100 g for a duration of 15 s, and 200 μ m spacings between indentations.

3. Results and discussion

3.1. Weld mechanical properties

During lap shear tensile test, the maximum loads before failure for RSW and URW joints are compared in Fig. 4. Overall, electrical current below 8.8 kA is insufficient to initiate welds, while too much expulsion is generated at and above 11 kA. According to AWS D8.1 M standard, the acceptable shear tensile strength (STS) of RSW welds can be calculated based on sheet thickness t (mm) and base metal tensile strength (TS, MPa) as the followings:

$$STS (kN) = \frac{\left[t^{1.5} \times (-2.544 \times UTS^3 \times 10^{-8} + 2.632 \times UTS^2 \times 10^{-5} + 6.696 \times UTS)\right]}{1000}_{min}$$

It can be seen that in the current conditions of 9.9 KA and 10.5 KA, all the welded samples are able to satisfy this minimum requirement of 10.5 kN and provide adequate joint mechanical strength. In this acceptable electrical current range, the difference between RSW and URW weld strength is insignificant statistically. RSW welds show slightly higher tensile shear strength. However, they failed in interfacial debonding (IF) mode, while all URW samples failed in nugget pull out (NPO) mode, as shown in Fig. 4.

To further show the different mechanical behaviors of URW and RSW welds in details, load displacement curves of welds obtained at 10.5 kA are provided in Fig. 5. In conventional RSW welds, a maximum load of 15.1 kN is reached, followed by a sharp drop in the curve, indicating a relatively brittle rapid failure. Interfacial debonding is generally observed, which agrees with the findings of Pouranvari and Marashi (2013) that AHSS steel welds are more prone to IF. As a comparison, the tensile load of the URW weld is slightly smaller at around 13.8 kN. However, nugget pullout mode (Fig. 4) is achieved with higher amount of plastic deformation. In other words, the weld is capable of absorbing more energy before failure. IF failure mode would

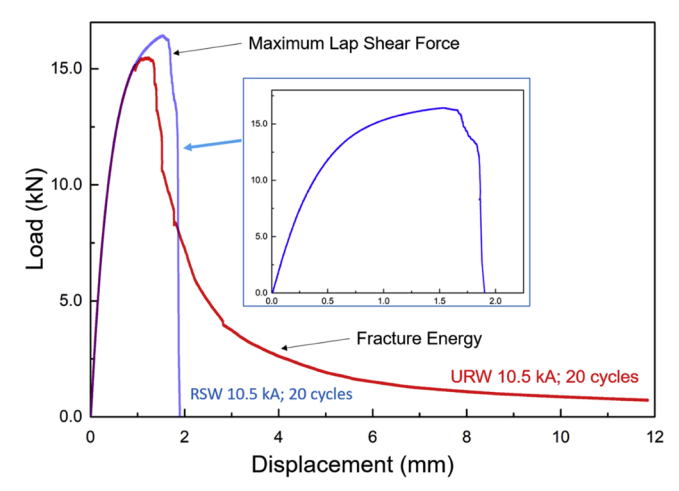


Fig. 5. Load displacement curve of RSW and URW welds obtained at 10.5 kA.

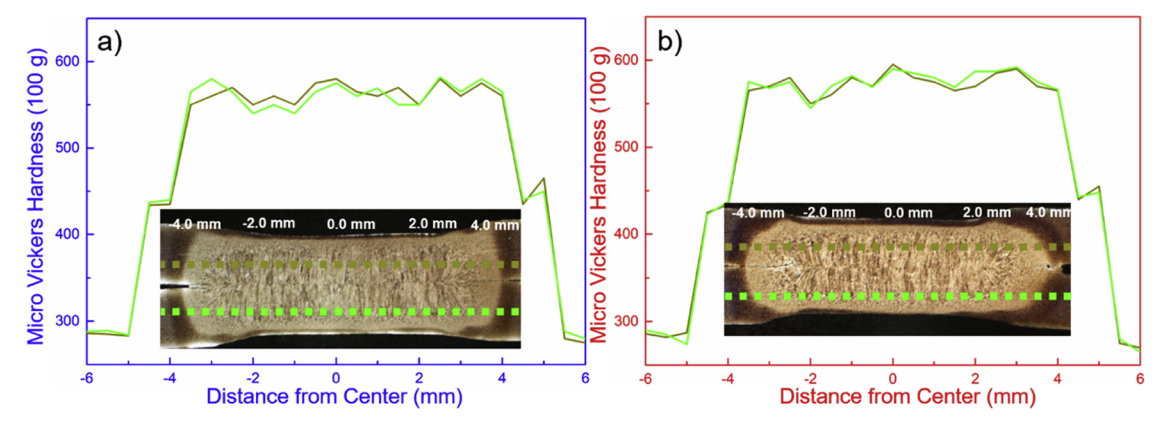


Fig. 6. Microhardness profile across the fusion zone a) RSW at 10.5 kA for 20 cycles b) URW at 10.5 kA for 20 cycles.

occur under the normal stress at the interface between the two sheets. During lap shear tensile tests, the notch tip of welds is initially loaded under mode II/III (tangential modes). As the weld starts to rotate, the fraction of mode I (normal opening) increases. Whereas in NPO, region around the weld fails due to the subjected tensile stresses arising from

the superimposed tension and bending loads. Fracture occurs in the relatively soft heat affected zone (HAZ). Microstructure comparison between the URW and RSW welds will be provided in the following session to understand these observed different mechanical behaviors.

To investigate the effects of Zn coating, another set of RSW welds

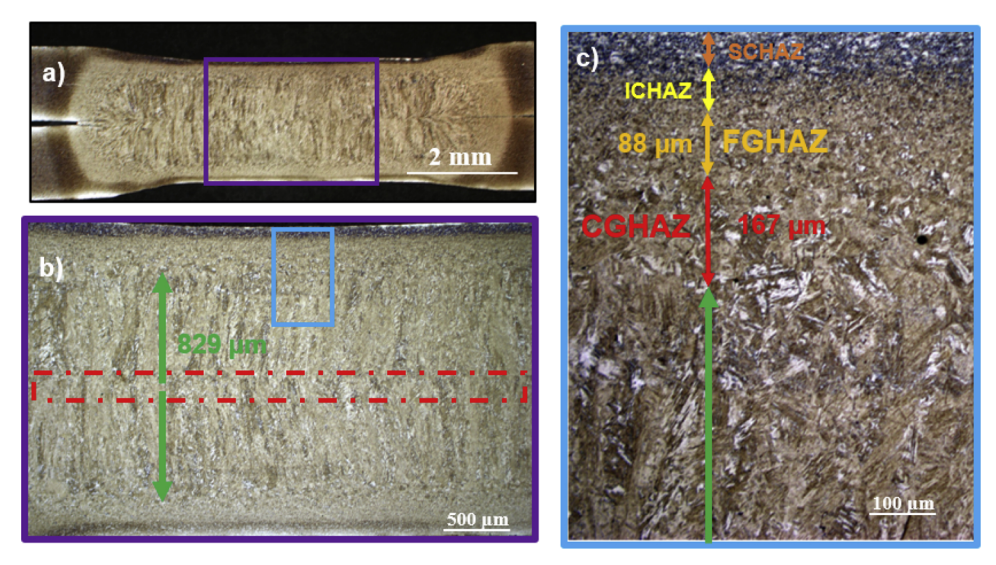


Fig. 7. Optical microscopic images of RSW welds at 10.5 kA for 20 cycles.

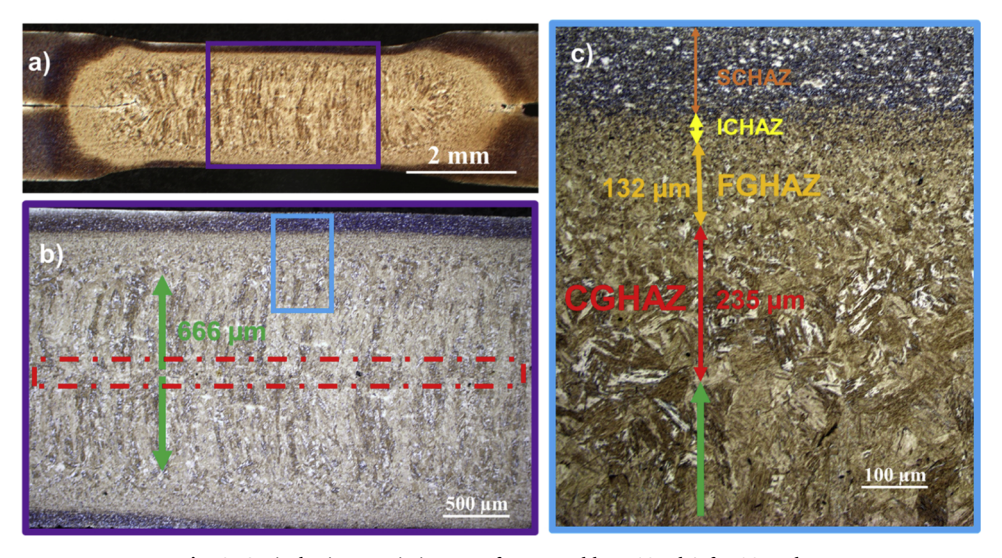


Fig. 8. Optical microscopic images of URW welds at 10.5 kA for 20 cycles.

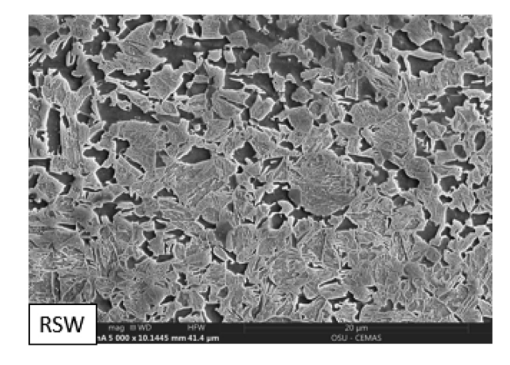


Fig. 9. SEM micrographs comparing ICHAZ between URW and RSW welds.

were performed where Zn layer was mechanically removed at the steel/steel contact interface prior to welding. In this case, NPO failure modes can be obtained for both URW and RSW welds. The Zn coating is known to have a lower electric resistance than bare TRIP steel. Lin et al. (2018) showed that as the thickness of the Zn layer increases, the weldability window would shift towards higher current region. Zn at the faying surface of the two sheets acts as an interface layer and tends to form a small weld nugget, which results in interfacial failure during tensile tests. In this investigation, removal of Zn shows the capability to transform the failure mode of RSW welds from IF to button pullout condition, which is similarly achieved through URW process, when all the electrical current parameters remain unchanged. Accordingly, it is hypothesized that the ultrasonic vibration can help break up the Zn coating at the contact interface during RSW, which facilitates weld nugget formation and growth.

Fig. 6 shows the microhardness profile from the base material (BM) towards fusion zone (FZ) along the center line. BM shows a relatively constant value of 280 HV. As the measurement point moves from base material towards the weld center, an intermediate increase of hardness can be observed, which is in the range of 425 HV to 435 HV and is located around 4 mm from the weld center. This is related to the inter critical heat affected zone (ICHAZ), which has a two-phase

microstructure consisting of ferrite and partially transformed martensite. Moving towards the fusion zone the hardness increases with the increasing fraction of martensite and bainite. The average hardness value of FZ is around 575 HV and the small amount of variations across the region is attributed to microstructural differences such as random distribution of martensitic and bainitic phase, different sizes and local crystallographic orientations of various grains, and possible local segregation of alloying elements.

3.2. Weld microstructure comparison

Microstructure of typical RSW and URW welds observed under a light optical microscope (LOM) is provided in Figs. 7 and 8 respectively. The welds are obtained under the condition of 10.5 kA, 20 cycles and welding force of 3.1 kN. Near the top and bottom surface of the workpiece that contacts electrodes, the subcritical heat affected zone (SCHAZ) is observed. In this region, the maximum temperature is below A1 and certain degree of bainite tempering and carbide coarsening can occur. Next to SCHAZ is the ICHAZ, where the peak temperature during welding is between A1 and A3. Austenitization will preferentially occur at martensite and bainite locations, which contain a higher carbon concentration. Subsequently during the fast cooling stage, these

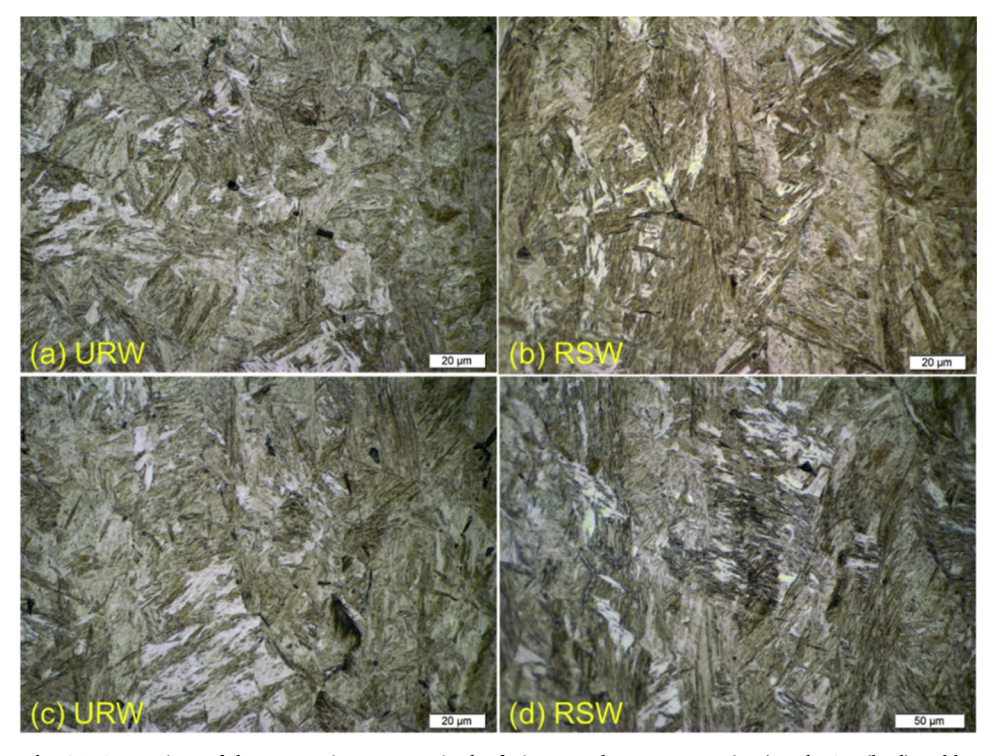


Fig. 10. Comparison of the martensite structure in the fusion zone between URW (a, c) and RSW (b, d) welds.

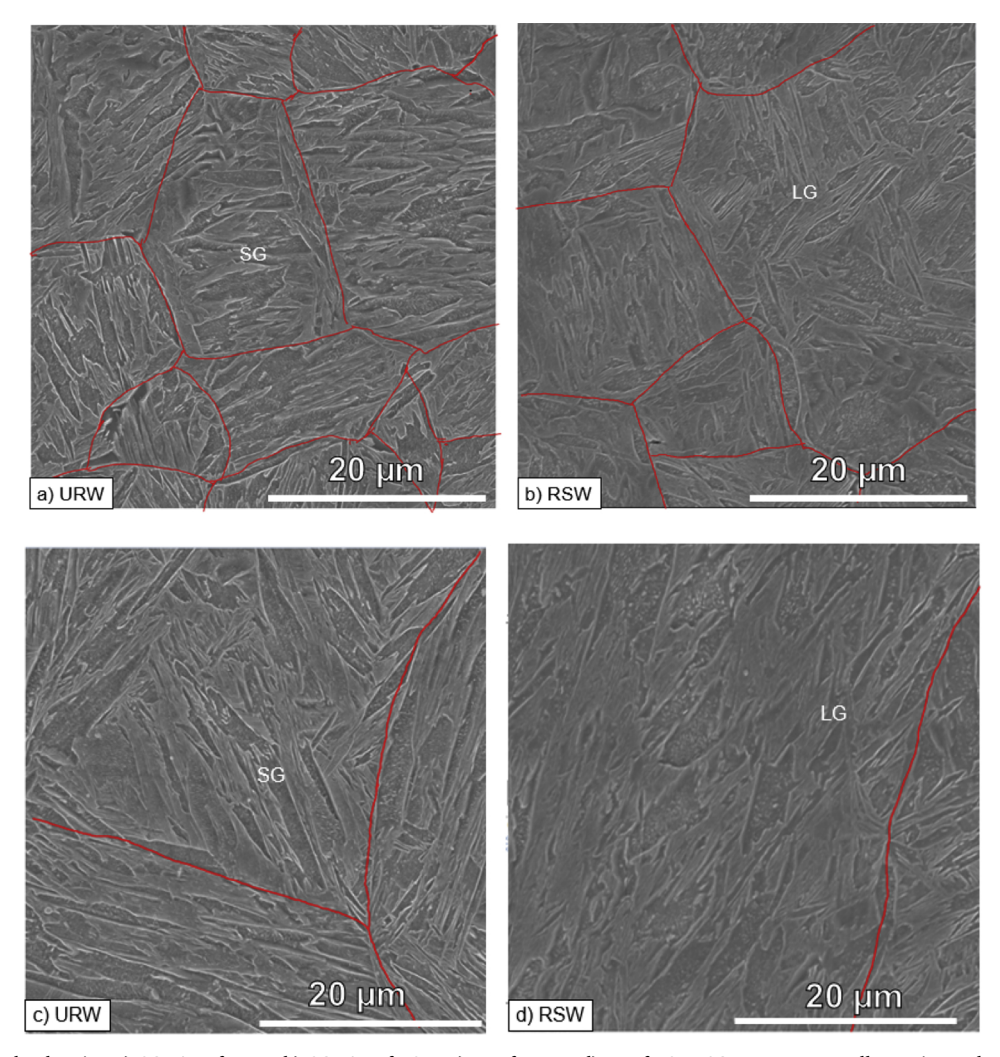


Fig. 11. SEM micrographs showing a) CGHAZ of URW; b) CGHAZ of RSW; c) FZ of URW; d) FZ of RSW. SG represents smaller grains and LG corresponds to larger grains.

partially transformed austenite will be more likely to form martensite due to carbon partitioning. As a result, ICHAZ consists of a two-phase structure including martensite and ferrite grains. SEM images of the ICHAZ zone in URW and RSW welds are compared in Fig. 9. The ICHAZ zone in URW welds is slightly narrower than that in RSW welds. Chen et al. (2009) previously calculated that ultrasonic energy can reduce alloy segregation at relatively high temperature. Accordingly, during URW process, the locally concentrated carbon in bainite and martensite regions can be homogenized under the superimposed ultrasonic vibration, which increases the average carbon level in the entire microstructure and facilities austenite transformation during heating stage. As a result, the amount of remaining ferrite is reduced, and the ICHAZ area is narrower.

In between ICHAZ and fusion zone (FZ) is the upper critical heat affected zone (UCHAZ), where the temperature is between A3 and the melting point. In this region, the base metal structure is fully transformed into austenite during heating, which eventually forms martensite and bainite upon cooling. Depending on the temperature range and length of thermal history, UCHAZ can be further divided into fine grain heat affected zone (FGHAZ) and coarse grain heat affected zone (CGHAZ). CGHAZ is located adjacent to the fusion zone. Large prior austenite grains can form in this region, which finally exhibit as blocky grains of martensite after the weld. Pouranvari and Marashi (2013) reported that the cooling rate of CGHAZ can be higher than FZ, which generally leads to a full martensite structure. The temperature in FGHAZ is relatively lower than CGHAZ and the transformed austenite

has a smaller grain size.

In the center of the weld is the fusion zone (FZ), where metal melting and solidification occurs. During RSW, the cooling rate can reach 4000 °C/s according to the calculations of Gould et al. (2006). This leads to directional epitaxial solidification towards the center of the fusion line, which forms large columnar structure of martensite and bainite along the thickness direction. The microstructure evolution in the fusion zone is dominantly controlled by peritectic solidification and solid-state eutectic phase transformation. It can be observed in Fig. 7 that in conventional RSW welds, the thickness of columnar martensitic grains in fusion zone (indicated by green arrow in Fig. 7b) is around 829 µm. As a comparison, after adding ultrasonic vibration, the thickness of this region is reduced by 20% to around 666 µm, shown in Fig. 8. Another interesting feature to observe is that in the RSW weld (Fig. 7b) the centerline along the weld thickness direction is sharp and straight while in case of URW, the centerline is not clearly distinguishable and is marked by the red dashed lines in Fig. 8b. The region where dendrites meet shows a zigzag behavior and entangle each other in a pattern of peaks and valleys. A more detailed comparison of the optical microstructure in the fusion zone between URW and RSW welds is provided in Fig. 10. More equiaxed structure and brighter (whitish) area can be observed in the URW welds.

The weld microstructure at different regions is further characterized with scanning electron microscope (SEM) for a higher magnified view. Fig. $11a\$ b compares the CGHAZ between URW and RSW welds, where the grains in the former one are smaller. Fig. $11c\$ d compares

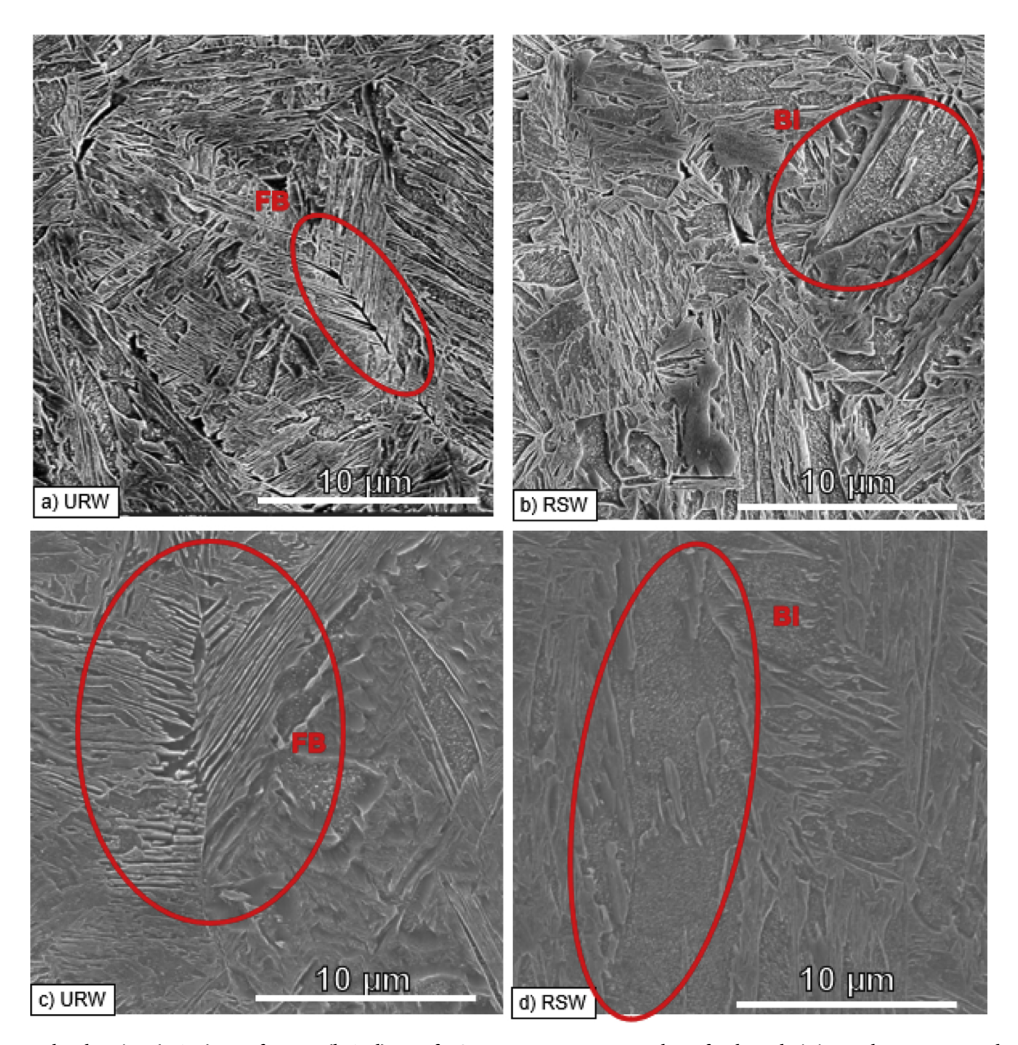


Fig. 12. SEM micrographs showing (a & c) FZ of URW; (b & d) FZ of RSW. Here FB corresponds to feathery bainite and BI corresponds to bainitic islands.

the fusion zone and a refined structure can also be observed in URW welds.

The fusion zone is further examined in detail, as shown in Fig. 12. Bainitic islands (BI) structure is observed in conventional RSW welds, which is also known as coalesced bainite, as studied by Keehan et al. (2005). Coalesced bainite has been found in dendritic core regions of AHSS welds. The formation of coalesced bainite starts with the supersaturated ferrite platelets with the same orientation, which join and merge into one coarse plate without intervening austenite film. Coalesced bainite is different from conventional lower bainite in terms of carbon precipitation. In coalesced bainite or BI, carbon is precipitated as cementite towards center of ferrite grain randomly, whereas in lower/upper bainite, cementite is present in certain pattern According to Keehan et al. (2006)and findings from other researchers, the presence of BI in the steel microstructure results in relatively high strength but poor toughness and less resistance to crack propagation. This agrees with our load displacement test results and the interfacial debonding failure mode observed in the RSW welds.

On the other hand, fusion zone of URW shows the presence of feathery bainite in certain locations, as in Fig. 12(a) and (c). According to Mehl (1939), feathery bainites are groups of large parallel ferrite plates formed during early stages of upper bainite.

Another interesting microstructure feature observed in URW welds is the possible existence of tempered martensite, as shown in Fig. 13a, c and d. In contrast, no evidence of tempering could be identified in the fusion zone of RSW welds, which is dominated by coalesced bainite. martensite is known to form through displacive transformation due to

fast cooling. Conventionally, martensite tempering is achieved by post processing heat treatments, where the specimen is held isothermally at elevated temperature to relieve the internal strain energy and allow diffusion of carbon atoms. The diffused carbon atoms would form precursor clusters within the solid solution. Upon further tempering, these precursor clusters will be able to transform into more stable cementite precipitates, shown as finely dispersed white particles in Fig. 13a, c and d. During URW process, it could be hypothesized that local absorption of ultrasonic energy at martensite laths facilitates carbon diffusion and cementite nucleation, resulting in certain degree of martensite tempering in the fusion zone.

3.3. Ultrasonic effects on RSW process

In the first several cycles of electrical current, the ultrasonic vibration possibly breaks up the Zn coating on the steel surface, which modifies the contact resistance and heat generation rate. After melting occurs, it can be expected that the ultrasonic energy is primarily absorbed by the molten pool in the fusion zone. The high intensity ultrasonic vibration is known to be capable of generating non-linear effects in liquids, including transient cavitation and acoustic streaming. These have been widely used for ultrasonic degassing of liquid metals to reduce porosity. Regarding the cavitation effect, micro-bubbles can be induced in the molten pool under the cyclic ultrasonic waves. During the negative pressure cycle, the micro bubbles grow while during the positive pressure cycle, they collapse implosively. This leads to instant local high pressure and temperature. During early stage of

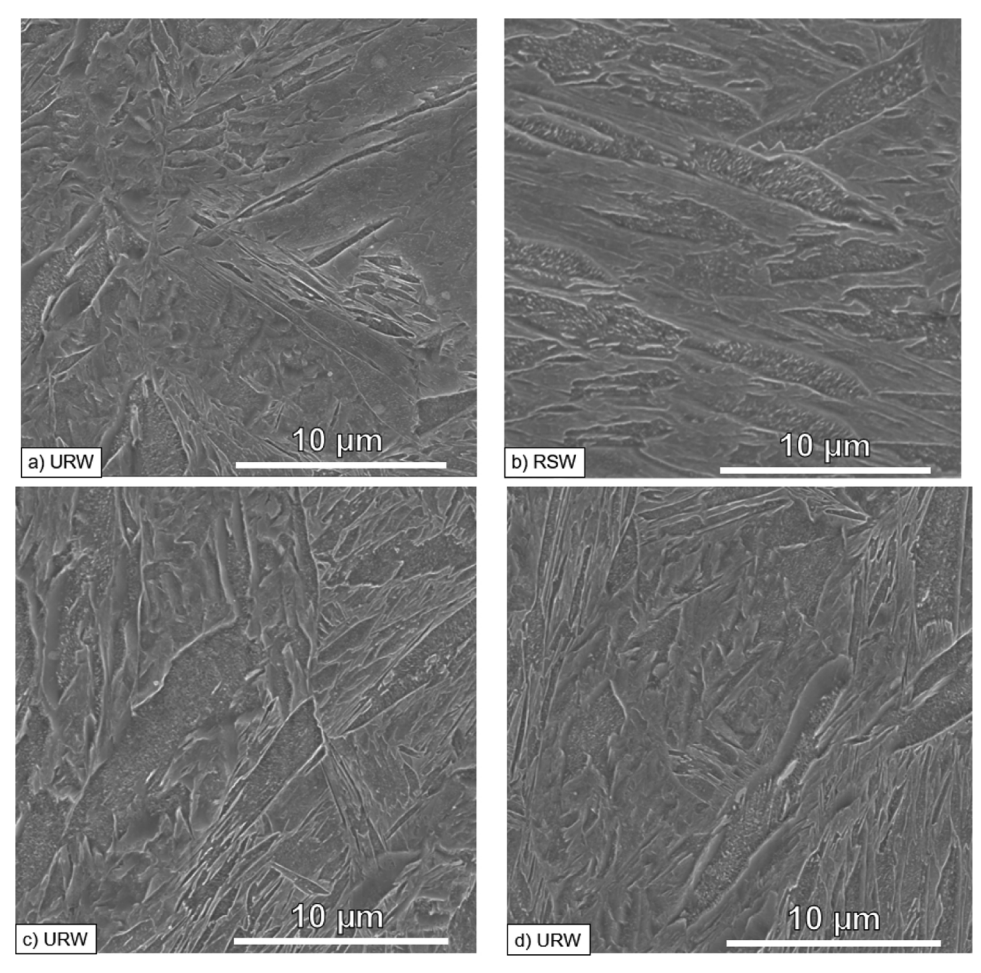


Fig. 13. SEM micrographs showing (a, c & d) FZ of URW; (b) FZ of RSW. In URW martensitic laths fine dispersion of white particles depicting cementite and representing tempering whereas in RSW large coalescence of bainite can be seen along with large martensitic laths. Also, the surface waviness and curvature depict another evidence of tempered microstructure.

solidification, ultrasonic induced cavitation disrupts the solidification front and fractures the large columnar dendrites and coarse prior austenite grains. During the collapse of bubbles from ultrasonic cavitation, microwaves and shock waves are generated on the solid surface and cause localized erosion, which is followed by dendrite defragmentation and promotes heterogeneous nucleation. Accordingly, the primary solidification structure can be refined to nearly equiaxed grains. This also partially explains the smaller thickness of fusion zone in the URW welds compared with RSW results. Acoustic streaming is a forced convection of material flow due to acoustic pressure gradients under the ultrasonic vibration. The associated high-speed flow in welding pool can effectively stir the material in microscopic scale, which improves the uniformity of element and temperature distribution. Moreover, the fragmented dendrite arms from cavitation effects could be carried away to new locations with acoustic streaming, which act as artificial sources of heterogeneous nuclei and form as new grains. This further refines the microstructure and promotes formation of the equiaxed structure, which can improve the ductility of URW welds compared with RSW welds. The refined URW microstructure is in agreement with the findings of the previous researchers when adding ultrasonic vibration into melting related manufacturing process. Kotadia et al. (2011) reported significant refinement of microstructure in the casted Al-Cu-Sn alloys due to ultrasonic irradiation. Also, Jian et al. (2005) reported the smaller grain size of aluminum A356 alloy in the presence of ultrasonic

In the final stage of cooling, potential martensite tempering takes place in URW. It is known that the martensite is thermodynamically unstable due to the large strain energy associated with carbon supersaturation in the BCT crystal lattice, as well as the high twin and dislocation density within the martensitic laths and along the lath interface. After the fusion zone is solidified, the continual supplied ultrasonic energy can be expected to be locally absorbed in these regions of high strain energy, such as dislocation rich sites in the martensite lath. The mechanism is similar to the material softening effect from acousto-plasticity. The local absorption of ultrasonic energy increases dislocations mobility and promotes dislocation annihilation, as was reported by Siu and Ngan (2011). The removed dislocation facilitates redistribution of carbon as they tend to segregate to the interstitial sites near dislocations, according to Speich and Leslie (1972). The redistributed carbon then precipitates out as cementite and other carbides, which results in ultrasonically assisted non-isothermal tempering of martensite. This tempered martensite reduces the brittleness of fusion zone and improves the ductility of URW welds in addition to the refined microstructure.

4. Conclusions

- During lap shear tensile tests, URW welds showed improved joint properties with nugget pullout failure mode, whereas RSW welds failed in the interfacial debonding mode.
- Ultrasonic vibration decreased the thickness of columnar dendritic martensitic region from $829\,\mu m$ to $666\,\mu m$ in the fusion zone and widens the heat affected zone area.
- Tempered martensite is observed in the fusion zone of URW welds,

which is potentially the result of local absorption of ultrasonic energy in martensite laths.

Acknowledgements

Authors would like to thank Matt Short from Edison Welding Institute for his assistance in tuning ultrasonic devices, Mai Huang from Arcelormittal for providing the TRIP steel sheets. Microstructure characterization works are supported by the OSU IMR grant 'Ultrasonic resistance spot welding of dissimilar materials'. The project is supported by National Science Foundation under the grant No. 1853632, An Innovative Hybrid Ultrasonic Resistance Welding Process for Joining Advanced Lightweight and Dissimilar Materials.

References

- Baltazar Hernandez, V.H., Panda, S.K., Okita, Y., Zhou, N.Y., 2010. A study on heat affected zone softening in resistance spot welded dual phase steel by nanoindentation. J. Mater. Sci. 45, 1638–1647. https://doi.org/10.1007/s10853-009-4141-0.
- Chen, Y.-J., Hsu, W.-N., Shih, J.-R., 2009. The effect of ultrasonic treatment on microstructural and mechanical properties of cast magnesium alloys. Mater. Trans. 50, 401–408. https://doi.org/10.2320/matertrans.MER2008273.
- Dancette, S., Massardier-Jourdan, V., Fabrègue, D., Merlin, J., Dupuy, T., Bouzekri, M., 2011. HAZ Microstructures and local mechanical properties of high strength steels resistance spot welds. ISIJ Int. 51, 99–107. https://doi.org/10.2355/isijinternational. 51.99.
- Ertek Emre, H., Kaçar, R., Ertek Emre, H., Kaçar, R., 2016. Resistance spot weldability of galvanize coated and uncoated TRIP steels. Metals (Basel) 6, 299. https://doi.org/10.3390/met6120299.
- Fan, Y.Y., Yang, C.L., Lin, S., Fan, C.L., Liu, W.G., 2012. Ultrasonic wave assisted GMAW: a novel method adds ultrasonic wave to provide an additional force to detach the droplet. Weld. J. https://www.files.aws.org/wi/supplement/WJ 2012 02 s91.pdf.
- Gallego-Juárez, J.A., Graff, K.F., 2015. Power Ultrasonics: Applications of High-Intensity Ultrasound. Woodhead Publishinghttps://doi.org/10.1016/B978-1-78242-028-6. 00001-6.
- Gould, J.E., Khurana, S.P., Li, T., 2006. Predictions of microstructures when welding automotive advanced high-strength steels. A combination of thermal and microstructural modeling can be used to estimate performance of welds in advanced highstrength steels. Weld. J. 85, 111s–116s. https://www.app.aws.org/wj/supplement/ WJ 2006 05 s111.pdf.
- Jian, X., Xu, H., Meek, T.T., Han, Q., 2005. Effect of power ultrasound on solidification of aluminum A356 alloy. Mater. Lett. 59, 190–193. https://doi.org/10.1016/J. MATIET 2004 09 027
- Jimma, T., Kasuga, Y., Iwaki, N., Miyazawa, O., Mori, E., Ito, K., Hatano, H., 1998. An application of ultrasonic vibration to the deep drawing process. J. Mater. Process. Technol. 80–81, 406–412. https://doi.org/10.1016/S0924-0136(98)00195-2.

- Keehan, E., Karlsson, L., Andrén, H.-O., Bhadeshia, H.K.D.H., 2006. Influence of carbon, manganese and nickel on microstructure and properties of strong steel weld metals: part 3 increased strength resulting from carbon additions. Sci. Technol. Weld. Join. 11, 19–24. https://doi.org/10.1179/174329306X77858.
- Keehan, E., Karlsson, L., Bhadeshia, H.K.D.H., 2005. Understanding mechanical properties of novel high strength steel weld metals through high-resolution microstructural investigations. Int. Conf. Trends Weld. Res. ASM Int. https://www.phase-trans.msm.cam.ac.uk/2005/coalesce.html.
- Kotadia, H.R., Das, A., Doernberg, E., Schmid-Fetzer, R., 2011. A comparative study of ternary Al-Sn-Cu immiscible alloys prepared by conventional casting and casting under high-intensity ultrasonic irradiation. Mater. Chem. Phys. 131, 241–249. https://doi.org/10.1016/J.MATCHEMPHYS.2011.09.020.
- Langenecker, B., 1966. Effects of ultrasound on deformation characteristics of metals. IEEE Trans. Sonics Ultrason 13, 1–8. https://doi.org/10.1109/T-SU.1966.29367.
- Li, X., Yang, Y., Cheng, X., 2004. Ultrasonic-assisted fabrication of metal matrix nanocomposites. J. Mater. Sci. 39, 3211–3212. https://doi.org/10.1023/B:JMSC. 0000025862.23609.6f.
- Lin, H.C., Hsu, C.A., Lee, C.S., Kuo, T.Y., Jeng, S.L., 2018. Effects of zinc layer thickness on resistance spot welding of galvanized mild steel. J. Mater. Process. Technol. 251, 205–213. https://doi.org/10.1016/J.JMATPROTEC.2017.08.035.
- Mehl, R., 1939. Hardenability of alloy steels. ASM Metals. pp. 41-44.
- Nagarajan, R., Dhanalakshmi, N.P., Krishnan, A., Sivakumar, V., Swaminathan, G., Goodson, M., 2006. Cavitation and acoustic streaming in ultrasonic fields: applications in bio-, leather-, and chemical processing. J. Acoust. Soc. Am. 119https://doi. org/10.1121/1.4786352. 3321–3321.
- Pouranvari, M., Marashi, S.P.H., 2013. Critical review of automotive steels spot welding: process, structure and properties. Sci. Technol. Weld. Join. 18, 361–403. https://doi. org/10.1179/1362171813Y.0000000120.
- Pouranvari, M., Marashi, S.P.H., 2011. Failure mode transition in AHSS resistance spot welds. Part I. Controlling factors. Mater. Sci. Eng. A 528, 8337–8343. https://doi. org/10.1016/J.MSEA.2011.08.017.
- Qian, Ma, Qian, M., Ramirez, A., 2014. Ultrasonic grain refinement of magnesium and its alloys titanium view project development of Ti64 TPMS gyroid structures via slm for orthopaedic implants view project ultrasonic grain refinement of magnesium and its alloys. Magnesium Alloys – Design, Processing and Properties. pp. 163–186. https:// doi.org/10.5772/560.
- Rezayat, H., Ghassemi-Armaki, H., Babu, S., 2016. Effects of heat affected zone softening extent on strength of advanced high strength steels resistance spot weld. 10th Int. Conf. Trends Weld. Res. https://doi.org/10.17605/OSF.IO/DH53G.
- Shi, C., Shen, K., Mao, D., Zhou, Y., Li, F., 2018. Effects of ultrasonic treatment on microstructure and mechanical properties of 6016 aluminium alloy. Mater. Sci. Technol. 34, 1511–1518. https://doi.org/10.1080/02670836.2018.1465514.
- Siu, K.W., Ngan, A.H.W., 2011. Understanding acoustoplasticity through dislocation dynamics simulations. Philos. Mag. 91, 4367–4387. https://doi.org/10.1080/14786435.2011.606237.
- Speich, G.R., Leslie, W.C., 1972. Tempering of steel. Metall. Trans. 3, 1043–1054. https://doi.org/10.1007/BF02642436.
- Xu, C., Sheng, G., Wang, H., Yuan, X., 2014. Reinforcement of Mg/Ti joints using ultrasonic assisted tungsten inert gas welding-brazing technology. Sci. Technol. Weld. Join. 19, 703–707. https://doi.org/10.1179/1362171814Y.0000000245.